# UCLA
## UCLA Previously Published Works

**Title**

Exchange of Cone for Rod Phosphodiesterase 6 Catalytic Subunits in Rod Photoreceptors Mimics in Part Features of Light Adaptation

**Permalink**

https://escholarship.org/uc/item/9r8641v7

**Journal**

Journal of Neuroscience, 35(24)

**ISSN**

0270-6474

**Authors**

Majumder, Anurima
Pahlberg, Johan
Muradov, Hakim
et al.

**Publication Date**

2015-06-17

**DOI**

10.1523/jneurosci.3563-14.2015

Peer reviewed

Cellular/Molecular

# Exchange of Cone for Rod Phosphodiesterase 6 Catalytic Subunits in Rod Photoreceptors Mimics in Part Features of Light Adaptation

**Anurima Majumder,**[1]* **Johan Pahlberg,**[3]* **Hakim Muradov,**[1]* **Kimberly K. Boyd,**[1] **Alapakkam P. Sampath,**[3] **and Nikolai O. Artemyev**[1,2]

[1]Department of Molecular Physiology and Biophysics and [2]Department of Ophthalmology and Visual Sciences, University of Iowa, Iowa City, Iowa 52242, and [3]Department of Ophthalmology, Jules Stein Eye Institute, University of California, Los Angeles, California 90095

Despite the expression of homologous phototransduction components, the molecular basis for differences in light-evoked responses between rod and cone photoreceptors remains unclear. We examined the role of cGMP phosphodiesterase (PDE6) in this difference by expressing cone PDE6 (PDE6C) in *rd1/rd1* rods lacking rod PDE6 (PDE6AB) using transgenic mice. The expression of PDE6C rescues retinal degeneration observed in *rd1/rd1* rods. Double-transgenic rods (PDE6C++) were compared with *rd1/+* rods based on similar PDE6 expression. PDE6C increased the basal PDE activity and speeded the rate-limiting step for phototransduction deactivation, causing rod photoresponses to appear light adapted, with reduced dark current and sensitivity and faster response kinetics. When PDE6C++ and *rd1/+* rods were exposed to similar background light, *rd1/+* rods displayed greater desensitization. These results indicate an increased spontaneous activity and faster deactivation of PDE6C compared with PDE6AB in darkness, but that background light increases steady PDE6C activity to a lesser extent. In addition to accelerating the recovery of the photoresponse, faster PDE6C deactivation may blunt the rise in background-induced steady PDE6C activity. Therefore, higher basal PDE6C activity and faster deactivation together partially account for faster and less sensitive cone photoresponses in darkness, whereas a reduced rise of steady PDE6C activity in background light may allow cones to avoid saturation.

*Key words:* cones; PDE6; phototransduction; retina; rods

---

### Significance Statement

Cones are the primary photoreceptors responsible for most of our visual experience. Cone light responses are less sensitive and display speeded responses compared with rods. Despite the fact that rods and cones use a G-protein signaling cascade with similar organization, the mechanistic basis for these differences remains unclear. Here, we examined the role of distinct isoforms of PDE6, the effector enzyme in phototransduction, in these differences. We developed a transgenic mouse model that expresses cone PDE6 in rods and show that the cone PDE6 isoform is partially responsible for the difference in sensitivity and response kinetics between rods and cones.

---

## Introduction

Most of our visual experience occurs during the day at light levels where cones are the primary active photoreceptor. Although

phototransduction research has focused largely on rods due to their quantum sensitivity (Pahlberg and Sampath, 2011), much less is known about cones. Cones are ∼100-fold less sensitive than rods and display photoresponses with a faster onset and recovery phase (Fu and Yau, 2007; Arshavsky and Burns, 2012; Korenbrot, 2012). Unlike rods, cones also do not saturate in

bright light and can adjust their responses to a wider range of background light intensities.

Rods and cones use a similar phototransduction pathway with cGMP as the second messenger gating transduction channels. The key signaling molecules—visual pigments (G-protein-coupled receptors), transducins (G-proteins), and phosphodiesterases-6 (effectors)—in rods and cones are represented by distinct yet highly homologous isoforms. Dissimilar light responses of rods and cones can be shaped by these components via control of a number of factors, including spontaneous phototransduction activity in the dark, signaling cascade coupling efficiency and amplification, rates of pigment and transducin/PDE6 inactivation, and strength of the $Ca^{2+}$-dependent feedback on the synthesis of cGMP during the recovery phase (Fu and Yau, 2007; Arshavsky and Burns, 2012; Korenbrot, 2012).

A rigorous test of the role of phototransduction components in rod/cone differences has been to compare the signaling by cone proteins in rods and vice versa. Such studies in *Xenopus* and mice have demonstrated that the signaling properties of rod and cone pigments are approximately equivalent (Kefalov et al., 2003; Shi et al., 2007, but see Sakurai et al., 2007). Furthermore, the difference in sensitivity of mammalian rods versus cones cannot be explained by the high spontaneous activation rate of the cone pigments (Fu et al., 2008). Studies on the role of transducin-$\alpha$ ($G\alpha_{t1}$) isoforms differ somewhat, but cumulatively point to a modest role in shaping photoresponses. For example, in one study, replacing $G\alpha_{t1}$ with the cone $G\alpha_{t2}$ in mouse rods decreased rod sensitivity and rate of activation while accelerating response recovery (Chen et al., 2010). Other studies concluded that $G\alpha_{t1}$ and $G\alpha_{t2}$ are functionally interchangeable in mouse rods (Deng et al., 2009; Mao et al., 2013). Finally, the differences in the flash response kinetics or in light adaptation of rods and cones may not be explained by the GCAP-mediated $Ca^{2+}$ feedback on cGMP synthesis (Sakurai et al., 2011).

PDE6 is a potential contributor to the differences in physiology of rods and cones. A recent study demonstrated that viral delivery of PDE6C could effectively rescue rod function using viral-mediated delivery of PDE6C to *rd10* rods (Deng et al., 2013). Surprisingly, the investigators found that PDE6C-expressing rods were more sensitive and slower to recover than wild-type (WT) rods (Deng et al., 2013), making them even more dissimilar from cones. It is known that the level of PDE6C expression, and thus basal PDE6 activity, is potentially a critical factor affecting photoreceptor sensitivity and response kinetics (Rieke and Baylor, 1996; Nikonov et al., 2000). However, Deng et al. (2013) did not assess the average PDE6C expression in injected *rd10* retinas compared with levels of rod PDE6 in WT retinas. Furthermore, they found that expression of PDE6C varied in individual *rd10* rods and some degree of retinal degeneration persisted. Here, we reexamined the hypothesis that PDE6 isoforms are essential contributors to the distinct physiology of rods and cones by generating transgenic mice expressing cone PDE6C in *rd1/rd1* rods lacking functional PDE6AB. Our results show that PDE6C expression rescues *rd1/rd1* rods from retinal degeneration. Furthermore, PDE6C confers dark-adapted rods with cone-like properties such as reduced sensitivity and accelerated response kinetics. Upon exposure to background light, however, *rd1/+* rods were desensitized to a greater extent than PDE6C++ rods, indicating lower steady PDE6 activity in PDE6C++ rods. The lower increase in steady PDE6C activity due to its faster deactivation may serve to prevent response saturation and increase the operational range of cones.

## Materials and Methods

*Generation of transgenic PDE6C+ and double-transgenic PDE6C++ mice.* To achieve reliable expression of the PDE6C transgene in mouse rods, we generated a transgenic construct with a spliceable intron between a 4.4 kb mouse opsin promoter and human PDE6C cDNA (see Fig. 1A). Such constructs function more like normal mammalian genes and often yield higher transgene expression in mice (Stec et al., 2001). A DNA fragment of 7.3 kb containing the transgene was microinjected into C57BL/6J × SJL/J mouse embryos at the University of Iowa transgenic core facility. Seven transgenic mouse founders were identified by PCR of mouse tail DNA and mated to C57BL/6J mice. Two founder lines expressing Flag-PDE6C were selected for breeding with homozygous *rd1/rd1* mice on a C57BL/6J background (B6.C3-*Pde6b^{rd1} le*) to produce single transgenic PDE6C+ mice. Initially, double-transgenic PDE6C++ mice with two PDE6C transgenic alleles were derived by inbreeding of PDE6C+ mice with subsequent identification through breeding with B6.C3-*Pde6b^{rd1} le* mice and genotyping of the progeny. However, our attempts to inbreed PDE6C++ mice have failed because PDE6C++ mice cannibalized their pups. Therefore, we proceeded to identify the transgene integration site to enable a genotyping-based selection of PDE6C++ mice resulting from breeding PDE6C+ mice. Mice of either sex were used in this study. All experimental procedures involving the use of mice were performed in accordance with the National Institutes of Health guidelines and the protocol approved by the University of Iowa Animal Care and Use Committee (Protocol #1208191).

*Identification of the transgene insertion site.* The PDE6C transgene integration site was determined by a procedure combining restriction enzyme digest of the genomic DNA with subsequent PCR amplification of an insertion site region (Bryda and Bauer, 2010). Because the 5′ end of the transgene with the mouse opsin promoter is not unique (see Fig. 1), only the 3′ end of the transgene insertion site sequence was amplified and analyzed. Three primers specific to the 3′-end of PDE6C cDNA were synthesized: primers 1 and 3 are the farthest and the closest to the unknown integration site, respectively. After digestion of tail-extracted genomic DNA with XbaI, SphI, HindIII, or SacI, a first round of linear PCR with primer 1 was conducted and the PCR mix was ligated overnight at 16°C with the Y-linker as described previously (Bryda and Bauer, 2010). A KpnI site is present at the 5′ end of the transgene. The Y-linker ligated products were digested with KpnI to avoid subsequent amplification of potential tail-to-head transgene junctions if multiple copies of the transgene were integrated. Second and third rounds of PCR were performed using primers 2 and 3, respectively, and reverse primers corresponding to the Y-linker. The third round yielded PCR products containing the 3′ region of the transgene fused to the genomic sequence of interest.

*Antibodies and immunoblotting.* Three types of anti-PDE6-peptide antibodies were custom made by Biosynthesis. Anti-PDE6C-specific antibodies were produced against mouse sequence PDE6C-157-175, which is identical in human and bovine PDE6C. Anti-PDE6A-specific antibodies were produced against mouse sequence PDE6A-31-50, matching the corresponding human and bovine sequences. Common PDE6 antibodies (PDE6com) that recognize PDE6C, PDE6A, and PDE6B equally well were generated against the GAFb sequence, which is highly conserved between all PDE6 subunits. All antibodies were immunoaffinity purified and the specificity was confirmed by immunoblotting. Total mouse retinal homogenates were obtained by solubilization of two retinas in 100 $\mu$l of 10% SDS-Na using brief sonication. Protein concentrations were determined using the DC Protein Assay (Bio-Rad) with bovine serum albumin dissolved in 10% SDS-Na serving as the standard. Samples of retinal homogenates were analyzed by immunoblotting using the following primary antibodies (1:1000 dilution): anti-PDE6C, anti-PDE6com, anti-PDE6A (Biosyntheis); anti-FLAG, anti-rod $G\alpha_{t1}$ (K-20), anti-$G\beta_1$ (M-14) (Santa Cruz Biotechnology); anti-phosducin (Sokolov et al., 2004); monoclonal anti-rhodopsin 1D4 (National Cell Culture Center); anti-PDE6AB MOE antibodies (Cytosignal); anti-arrestin (PA1-731; ABR); and anti-RGS9 antibodies (Elmira Biologicals). Levels of PDE6C were quantified by measuring the integrated densities of the bands using ImageJ.
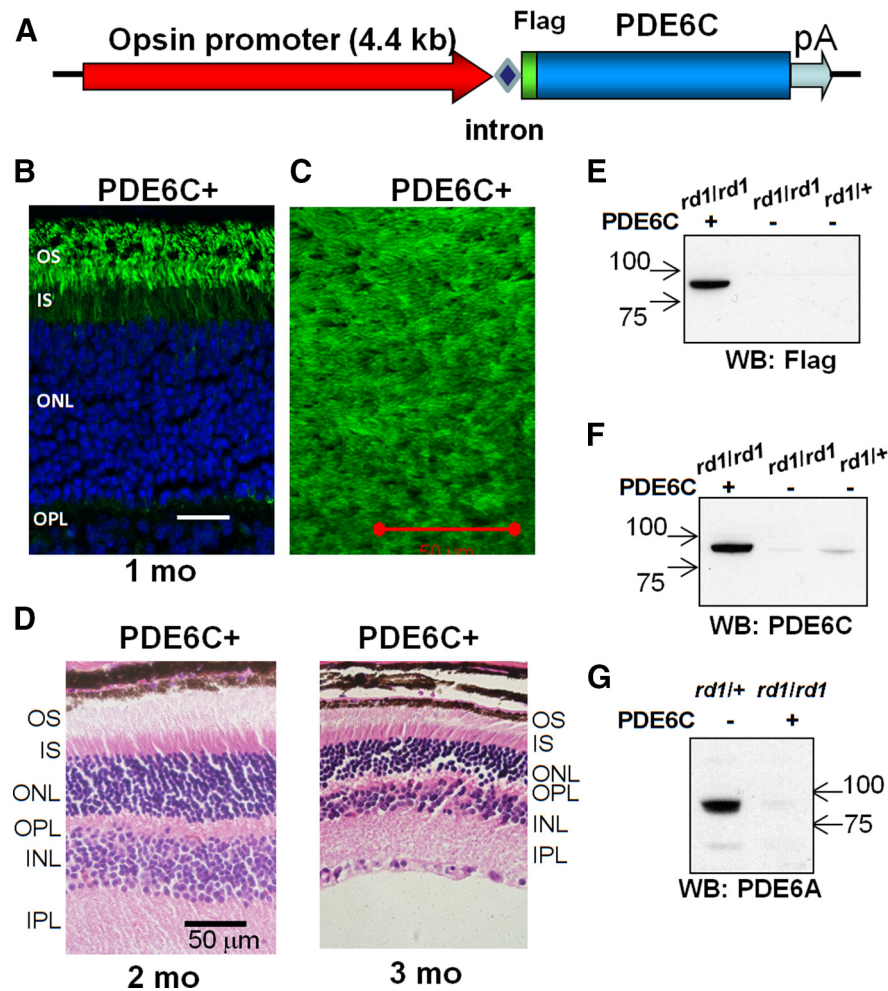
**Figure 1.** Expression and localization of PDE6C in PDE6C+ mouse retina. **A**, Transgenic construct for generation of PDE6C+ mice. **B**, PDE6C in transgenic rods is correctly targeted to the OS. Retina cryosections from PDE6C+ mice were stained with a rabbit anti-FLAG antibody (green). Blue is TO-PRO3 nuclear stain. IS, Inner segments; ONL, outer nuclear layer; OPL, outer plexiform layer; INL, inner nuclear layer; IPL, inner plexiform layer. Scale bar, 20 $\mu$m. **C**, Retina flat-mount immunofluorescence imaging (Flag, green). Scale bar, 50 $\mu$m. **D**, Retina morphology of 2- and 3-month-old PDE6C+ mice. Paraffin sections of the PDE6C+ retina were stained with H&E. Scale bar, 50 $\mu$m. **E–G**, Transgenic PDE6C and endogenous PDE6A and PDE6C levels were analyzed by Western blotting in retinas of 1-month-old PDE6C+ and nontransgenic (PDE6C−) mice in the *rd1/+* and *rd1/rd1* backgrounds using anti-FLAG (**E**), PDE6C (**F**), and PDE6A (**G**) antibodies.

*Retinal morphology and immunofluorescence.* Mice were euthanized by $CO_2$ asphyxiation, eyes were enucleated, poked through the cornea with a 21 gauge needle, and fixed in 4% paraformaldehyde in PBS for 1 h at 25°C. The eyes were then cut to remove the cornea and the lens and the eyecups were transferred back to 4% paraformaldehyde in PBS and fixed overnight at 4°C. The eyecups were embedded in paraffin, sectioned (Leica RM2135), and stained with H&E. These retinal sections were subsequently examined using an Olympus BX51 microscope with 40× magnification. Cryosections of mouse retina were obtained and stained with anti-FLAG antibody, followed by staining with goat anti-mouse Alexa Fluor 488 secondary antibodies as described previously (Sinha et al., 2013).

In experiments to establish the spatial expression of PDE6C across the retina (see Fig. 1C), whole mouse eyes were enucleated under red light, leaving a section of the optic nerve attached to the eye, and the dorsal side was marked by puncturing the cornea with a 21 gauge needle. The whole eye was fixed in 4% paraformaldehyde in 1× PBS for 30 min. The eye was then removed from fixative and the lens and cornea were cut and removed to make an eyecup. The retina was carefully isolated from the retinal pigment epithelium and free-floating retinas were fixed in 4% paraformaldehyde for another 6 h. The tissue was then stained with anti-FLAG antibody, followed by staining with goat anti-mouse Alexa

Fluor 488 secondary antibodies as described previously (Sinha et al., 2013). Before imaging, the retina was placed on a Superfrost Plus slide (Fisher Scientific) with the outer segments (OS) of the photoreceptor cells facing up. Radial cuts were made to flatten the tissue before mounting it gently with a coverslip, taking care not to damage the structure of the outer retina.

*Assays of PDE6 activity and inhibition by Pγ-subunits.* Typically, 2–4 mouse retinas were homogenized under dim red light by sonication (2 s pulses, 3 times) in 200 $\mu$l of 20 mM Tris-HCl, pH 7.5, buffer containing 120 mM NaCl, 1 mM $MgSO_4$, and 1 mM $\beta$-mercaptoethanol. An aliquot of the homogenate was used to determine rhodopsin concentration, whereas the remaining portion, after brief centrifugation (3000 × g, 2 min) to remove cell debris, was used to measure the basal and maximal (trypsin-activated) PDE6 activities. Rhodopsin concentration was determined from the absorption spectra before and after complete bleaching of the sample in 3% lauryldimethylamine N-oxide in 1× PBS using an extinction coefficient at 500 nm of 42,000 $M^{-1}$ $cm^{-1}$. Trypsin-activated PDE activities were measured using the proton-evolution assay (Liebman and Evanczuk, 1982). The assay was performed at 25°C in a final volume of 200 $\mu$l in 10 mM-HEPES buffer, pH 8.0, containing 100 mM KCl, 2 mM $MgCl_2$, and 1 mM DTT. The reaction was initiated by the addition of retinal homogenate (~0.1 $\mu$M rhodopsin), trypsin (20 $\mu$g/ml), and cGMP (4 mM). The pH was monitored with a pH microelectrode (Microelectrodes). Basal PDE6 activity was measured using [$^3$H]cGMP as described previously (Muradov et al., 2006). Briefly, retinal homogenates (~0.03 $\mu$M rhodopsin) were incubated in 40 $\mu$l of 20 mM Tris-HCl, pH 7.5, buffer containing 120 mM NaCl, 2 mM $MgSO_4$, 1 mM 2-mercaptoethanol, 0.1 U bacterial alkaline phosphatase, and 10 $\mu$M [$^3$H]cGMP (100,000 cpm) for 10 min at 25°C. The reaction was stopped by the addition of AG1-X2 cation exchange resin (0.5 ml of 20% bed volume suspension). Samples were incubated for 6 min at 25°C with occasional mixing and centrifuged at 10,000 × g for 3 min. Finally, 0.25 ml of the supernatant was removed for counting in a scintillation counter. Groups of measurements were compared with two-tailed unpaired t test.

For Pγ-inhibition assays, ROS preparations were isolated from PDE6C+ and WT mouse retinas as described previously (Tsang et al., 1998). Trypsin-treated PDE6C and PDE6AB were obtained by incubating ROS suspensions (7–8 $\mu$M rhodopsin) with trypsin (100 $\mu$g/ml) for 10 min at 25°C, followed by the addition of a 5-fold excess of soybean trypsin inhibitor. The membranes were pelleted by centrifugation (100,000 × g, 60 min) and the supernatants were stored in 40% glycerol at −20°C until use. PDE activity was measured using 5 $\mu$M [$^3$H]cGMP and 1 pM PDE6 (Hamilton et al., 1993; Muradov et al., 2006) in the absence or presence of the indicated concentrations of purified recombinant Pγr and Pγc. The $K_i$ values for PDE6 inhibition by Pγ were calculated by fitting data to equation: $Y(\%) = 100/(1 + 10^\wedge(X - \mathrm{Log}K_i))$, where X is the logarithm of total Pγ concentration. Fitting the experimental data to equations was performed with nonlinear least-squares criteria using GraphPad Prism software.

*Physiological recordings from rod photoreceptors.* The rod OS photocurrent was assessed either with suction electrodes from dissociated dark-adapted retinal tissue (Okawa et al., 2010) or by whole-cell patch clamp

recordings ($V_m = -40$ mV) from rod photoreceptors in dark-adapted slices of the mouse retina (Okawa et al., 2008; Majumder et al., 2013). Briefly, mice were dark adapted overnight and euthanized in accordance with a protocol approved by the University of California–Los Angeles Animal Research Committee (Protocol # 14–005). All manipulations were performed under infrared illumination with infrared image-converting goggles. Eyes were enucleated, dissected into eyecups, and stored in darkness at 32°C in bicarbonate-buffered Ames' medium equilibrated with 5% $CO_2$/95% $O_2$.

Suction recordings were made from pieces of retina separated from the eyecup, chopped into small pieces, and placed into a recording chamber that was superfused with bicarbonate-buffered Ames' medium equilibrated with 5% $CO_2$/95% $O_2$ and maintained at 35–37°C. Light-evoked responses to 20 ms flashes were generated by a shutter-controlled lamp projected through a 500 nm interference filter. Data were sampled at 100 Hz and low-pass filtered at 30 Hz.

To make patch-clamp recordings from rods, the retina was separated from the eyecup, embedded in low-gelling-temperature agar (Sigma A-0701), and tissue slices were cut on a vibrating microtome (Leica VT-1000S). Tissue slices were placed in a recording chamber and superfused with bicarbonate-buffered Ames' medium maintained at 35–37°C, and equilibrated with 5% $CO_2$/95% $O_2$. Light-evoked responses were generated by 10 ms flashes from a blue light-emitting diode ($\lambda_{max} \sim 470$ nm) the strength of which was varied. Data were sampled at 1 kHz and low-pass filtered at 300 Hz.

Average dim flash responses were calculated as the weighted average of all linear range responses ($< 25\%$ maximum amplitude). Light sensitivity was estimated as the flash strength that produced a half-maximal response ($I_{1/2}$) based on the fit of a saturating exponential function through the data (Lamb et al., 1981). In experiments to assess light adaptation, a second light-emitting diode's output produced the background light. Light intensities were converted to $R^*$/rod based on estimates of the rod OS collecting area in each genotype (see Fig. 5B).

## Results

### PDE6C is targeted correctly to rod OS and rescues *rd1/rd1* retinal degeneration in a transgenic mouse model

A small, nine-residue Flag tag was added to the N terminus of human PDE6C (Fig. 1A) to facilitate detection of the transgene expression before breeding transgenic mice into the *rd1/rd1* background. The N-terminal tag was not expected to influence the structure and function of PDE6C because the extreme N terminus is not conserved in PDE6 enzymes and has no known function. Immunofluorescence analysis of the transgenic retina in the *rd1/rd1* background (PDE6C+) revealed that Flag-PDE6C is expressed in rods and is correctly targeted to the OS (Fig. 1B). Whole-mount immunofluorescence imaging

**PDE6C++**

**PDE6C++**

OS
IS
ONL
OPL
INL
IPL

***rd1*/+ PDE6C++**

WB: Flag

WB: PDE6C
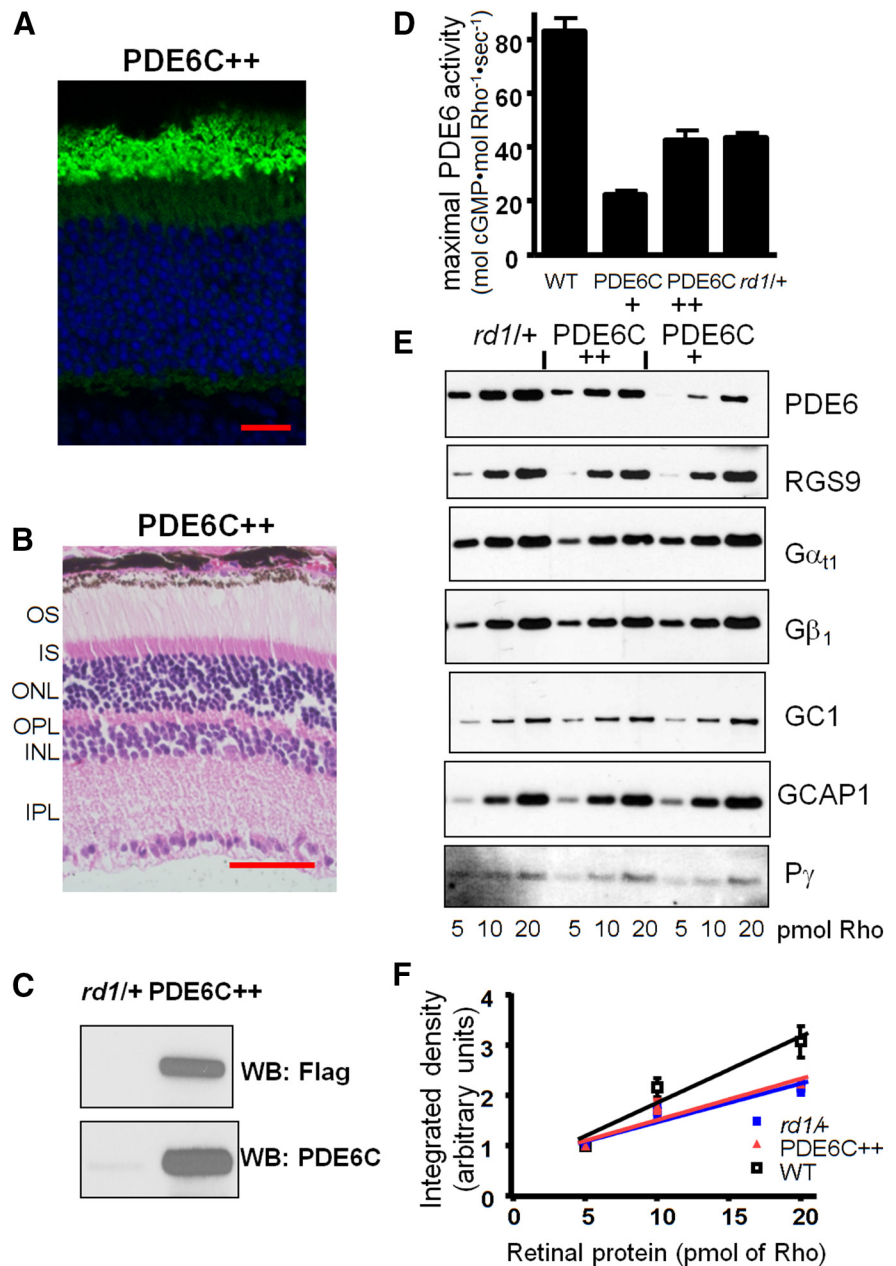
**Figure 2.** Characterization of double-transgenic PDE6C++ mouse retina. ***A***, Retina cryosections from PDE6C++ mice were stained with a rabbit anti-FLAG antibody (green). Blue is TO-PRO3 nuclear stain. Scale bar, 20 μm. ***B***, Retina morphology of 3-month-old PDE6C++ mice. Paraffin sections of the PDE6C++ retina were stained with H&E. Scale bar, 50 μm. ***C***, Transgenic and endogenous PDE6C levels were analyzed by Western blotting in retinas of 3-month-old PDE6C++ and *rd1*/+ mice. ***D***, Maximal (trypsin-simulated) PDE6 activities in rhodopsin-normalized retinal homogenates from WT, *rd1*/+, PDE6C+, and PDE6C++ mice were measured using a proton-evolution assay. ***E***, Retinal homogenates from *rd1*/+, PDE6C+, and PDE6C++ mice were analyzed by Western blotting. The antibodies used are described in Materials and Methods. ***F***, Levels of PDE6 catalytic subunits were quantified by measuring the integrated densities of the bands from Western blots with PDE6com antibodies using ImageJ. Linear fits were obtained using normalized integrated densities from 3 separate experiments (mean ± SEM, $n = 3$). From this analysis, PDE6 protein levels in the PDE6C++ and *rd1*/+ samples are similar and ~2-fold lower than in the WT retinal homogenate.

showed uniform transgenic expression of PDE6C (Fig. 1C). Importantly, the introduction of the PDE6C transgene rescued retinal degeneration in 2-month-old *rd1/rd1* mice (Fig. 1D), suggesting that PDE6C is functional in transgenic rods. The immunoblot analysis of PDE6C+ retina with anti-Flag antibodies demonstrated expression of the PDE6C band of appropriate size in these animals, which was not present in either *rd1*/+ or *rd1/rd1* mice (Fig. 1E). The levels of transgene expression in PDE6C+
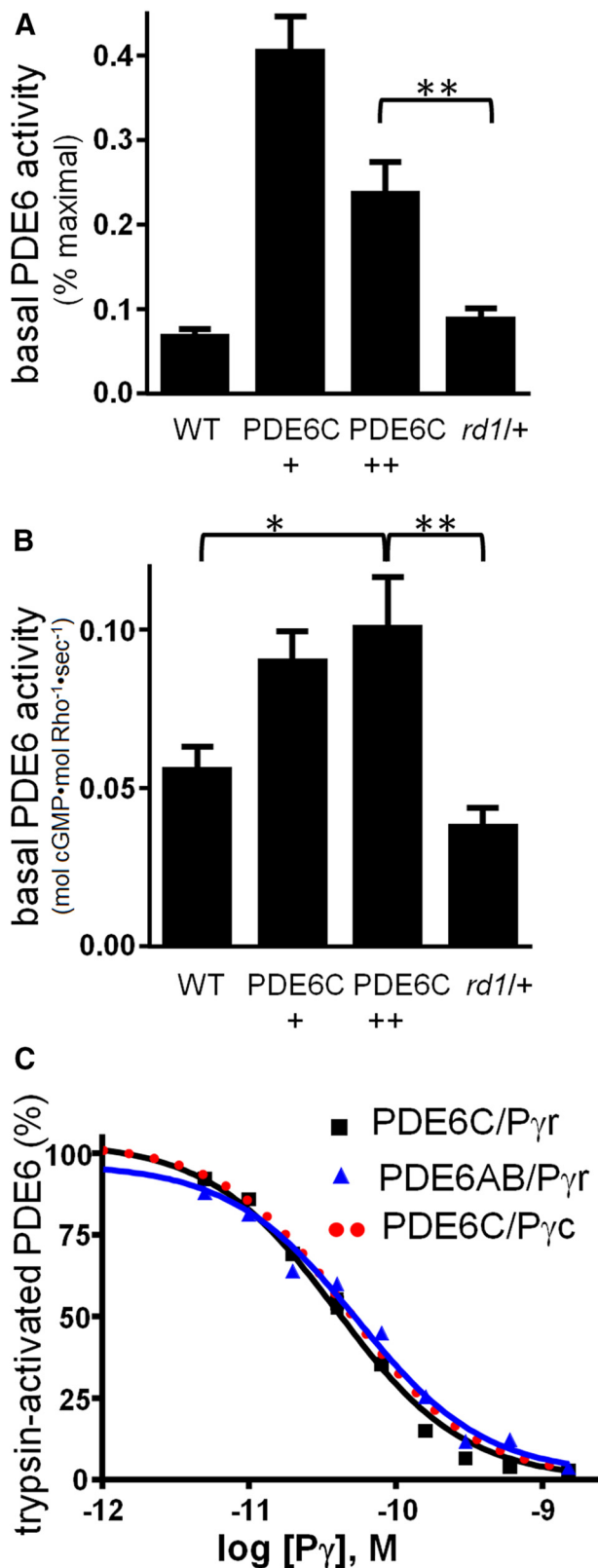
**Figure 3.** Elevated basal PDE6C activity in transgenic mice. *A*, Basal PDE6 activities in retinal homogenates from WT, *rd1/+*, PDE6C+, and PDE6C++ mice are expressed as fractions of the respective maximal trypsin-activated PDE6 activities. **$p = 0.006$; $n = 5$. *B*, Basal PDE6 activities in retinal homogenates from WT, *rd1/+*, PDE6C+, and PDE6C++ mice normalized to rhodopsin levels. *$p = 0.034$; **$p = 0.006$; $n = 5$. *C*, Trypsin-activated PDE6C and PDE6AB obtained from mouse ROS fractions were inhibited by Pγr with the $K_i$ values of 40 and 43 pM, respectively. For comparison, inhibition of similarly obtained trypsin-activated PDE6C by Pγc is shown as dotted line ($K_i = 47$ pM). Results from representative experiments are shown.

mice are markedly higher than the level of native PDE6C in control *rd1/+* retinas as judged by immunoblotting with PDE6C-specific antibodies (Fig. 1*F*). Native PDE6C is almost undetectable in *rd1/rd1* retinas due to retinal degeneration (Fig. 1*F*). PDE6C+ mice in the *rd1/rd1* background may express PDE6A. In *rd1/rd1* mice, before degeneration, PDE6A is reduced and nonfunctional (Tsang et al., 1996), apparently due to lack of dimerizing partner PDE6B. In PDE6C+ mice, the levels of PDE6A were barely detectable (Fig. 1*G*), suggesting that PDE6A does not dimerize with PDE6C and is degraded.

### Levels of PDE6C expression and maximal activity in PDE6C+ and PDE6C++ rods

Despite the normal appearance of the PDE6C+ retina in 2-month-old mice, we observed thinning of the OS and the outer nuclear layer in 3-month-old mice (Fig. 1*D*). This observation was supported by the measurements of rhodopsin content in the eye (Majumder et al., 2013), which showed an ~45% reduction of rhodopsin levels in 3-month-old PDE6C+ mice [370 ± 15 pmol/eye; $n = 5$ compared with 680 ± 25 pmol/eye in WT (C57BL) mice; $n = 4$]. Immunoblotting with PDE6com antibodies revealed that the level of PDE6C in PDE6C+ retinas normalized to rhodopsin content was ~4-fold lower compared with PDE6AB expression in WT retinas (data not shown). In agreement, the maximal PDE6 activity measured in the PDE6C+ and WT retina homogenate after limited trypsinization was also proportionally lower for the transgenic mice (Fig. 2*D*).

To achieve equivalent levels of PDE6C in rods of mutant mice and PDE6AB in control rods, we generated double-transgenic PDE6C++ mice with two PDE6C transgenic alleles and evaluated heterozygous *rd1/+* mice as controls. We identified the transgene insertion site to enable selection of PDE6C++ mice resulting from breeding PDE6C+ mice by genotyping. The PDE6C transgene integrated into chromosome 4 at ~8 kbp from the 5′ side of the Ubxn2b gene (UBX-domain containing protein B2) and ~44 kbp from the 3′ side of Cyp7a1 gene (cholesterol 7-α-monooxygenase). Therefore, the transgene insertion did not disrupt any gene essential for phototransduction or photoreceptor function. PDE6C++ retinas showed proper targeting of PDE6C to the OS (Fig. 2*A*), normal morphology (Fig. 2*B*), and robust levels of PDE6C protein (Fig. 2*C*) in 3-month-old mice. The rhodopsin level in 3-month-old PDE6C++ mice (570 ± 25 pmol/eye; $n = 4$) was also improved significantly from that in PDE6C+ mice. Rhodopsin-normalized expression of PDE6C doubled in PDE6C++ mice, as assessed by maximal PDE6 activity (Fig. 2*D*) and by the Western blotting (Fig. 2*E,F*). The strong gene dosage effect seen in PDE6C+ and PDE6C++ mice was also evident in *rd1/+* mice. PDE6AB protein levels, as well as maximal PDE6 activity in *rd1/+* retinas, were decreased by about 2-fold compared with the WT values (Fig. 2*D,F*). As a result, PDE6 protein expression and maximal catalytic activity were similar in *rd1/+* and PDE6C++ mice (Fig. 2*D*–*F*). Rhodopsin levels in 3-month-old *rd1/+* mice (620 ± 50 pmol/eye; $n = 4$) and PDE6C++ mice were not different ($p = 0.41$). The levels of the other major phototransduction proteins were similar in the two mouse lines as well (Fig. 2*E*). Therefore, *rd1/+* mice were selected as appropriate controls for PDE6C++ mice for further analysis.

### Basal PDE6 activity is elevated in rods expressing PDE6C

Basal PDE6 activity is a key factor influencing the sensitivity and kinetics of photoreceptor responses (Rieke and Baylor, 1996; Nikonov et al., 2000). We examined the levels of basal PDE6
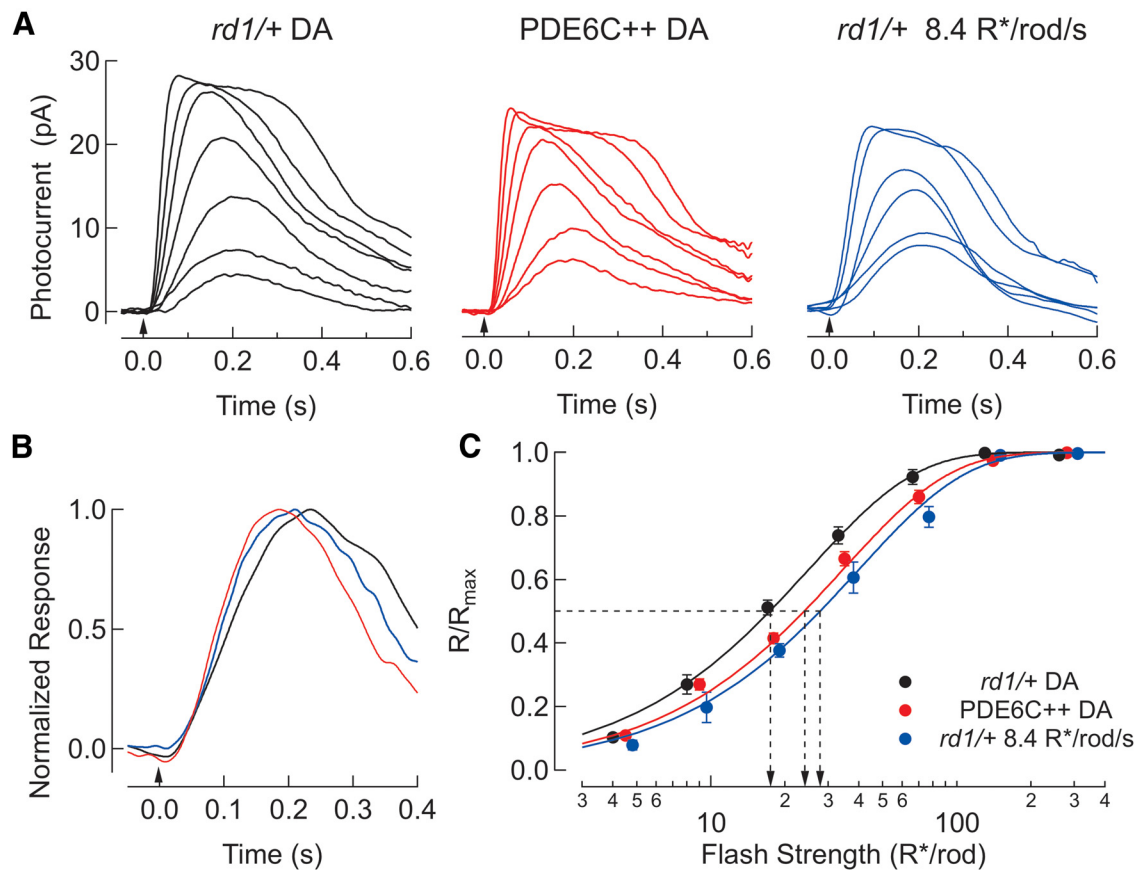
**Figure 4.** Physiological responses of PDE6C++ and rd1/+ rods. **A.** Light-evoked responses of rd1/+ and PDE6C++ rods in darkness (DA) collected in whole-cell voltage clamp ($V_m = -40$ mV). Flash responses of a representative rd1/+ rod that (black) yielded 3.4, 6.7, 14, 28, 55, 110, and 220 R*/rod; a representative PDE6C++ rod (red) that yielded 3.8, 7.6, 15, 29, 59, 120, and 240 R*/rod; and a representative rd1/+ rod exposed to 8.4 R*/rod/s (blue) that yielded 8.1, 16, 32, 65, 130, and 260 R*/rod. The timing of the flash is denoted by an arrow. Rod responses were sampled at 1 kHz and further low-pass filtered at 30 Hz. **B,** Average normalized dim flash response (<25% $R_{max}$) of rd1/+ (black) and PDE6C++ rods (red) and of rd1/+ rods exposed to a background light yielding 8.4 R*/rod/s (blue). The average response was produced by 3.4 R* in rd1/+ rods (n = 37 responses), 3.8 R* in PDE6C++ rods (n = 26 responses), and 4.2 R* in rd1/+ rods exposed to 8.4 R*/rod/s (n = 15 responses). **C,** Normalized average response-intensity relationship for rd1/+ (n = 9; mean ± SEM) and PDE6C++ rods (n = 10; mean ± SEM) in darkness, and rd1/+ rods exposed to 8.4 R*/rod/s background light (n = 5; mean ± SEM). Each dataset was fit with an exponential saturation function (Lamb et al., 1981) from which the $I_{1/2}$ value was extracted. The $I_{1/2}$ values for this fit were 17 R*, 24 R*, and 28 R* for rd1/+, PDE6C++, and rd1/+ rods exposed to 8.4 R*/rod/s, respectively. Dashed horizontal line reflects $I_{1/2}$ to allow a comparison of sensitivity across genotypes and conditions (see also Table 1).

activity in retinas of WT, PDE6C+, PDE6C++, and rd1/+ mice. Basal rod PDE6 activities as fractions of the respective maximal trypsin-activated activities were similar and very low in WT and rd1/+ mice (Fig. 3A), consistent with previous studies (Tsang et al., 1998). However, the basal activities of cone PDE6C in PDE6C+ and PDE6++ retinas constituted significantly larger fractions of the respective maximum levels (Fig. 3A). Particularly, the basal activity in PDE6C++ retinas was almost 3-fold higher than the basal activity in rd1/+ retinas containing equivalent PDE6 protein levels. The reason for the higher basal PDE6 activity in PDE6C+ retina homogenates versus PDE6C++ is unclear (Fig. 3A). This difference may be due to low levels of PDE6C in PDE6C+ retina or to the ensuing retinal degeneration. Basal PDE6 activities normalized to maximal activity (i.e., PDE6 content) reflect the intrinsic property of the enzyme. However, normalization to rhodopsin may better represent the ratios of basal activity levels in control and mutant rods, because the amount of rhodopsin correlates with the cumulative OS volume in which cGMP is hydrolyzed. The basal PDE6 activity normalized to rhodopsin levels is also significantly higher in PDE6C++ samples than in rd1/+ or WT samples (Fig. 3B).

In transgenic rods, PDE6C is complexed with the rod-specific Pγr inhibitory subunit, which is homologous but not identical to the cone-specific Pγc. We investigated whether the difference in the basal PDE6 activities in PDE6C++ and rd1/+ retinas is due to different affinities of PDE6C and PDEAB for Pγr. Trypsin-activated PDE6C and PDE6AB were equipotently inhibited by Pγr with $K_i$ values that were not different from the $K_i$ value for PDE6C inhibition by Pγc (Fig. 3C).

**Rods of PDE6C++ mice are desensitized compared with rd1/+ controls**

The basal PDE activity in rod OS is a key parameter that controls the sensitivity and time course of rod photoresponses. The higher basal PDE activity in PDE6C++ retinas compared with rd1/+ mice suggests that light-evoked responses in PDE6C++ rods may be accelerated. We characterized the functional properties of light-evoked responses by recording from dark-adapted rods in retinal slices using patch clamp recordings. Typical responses for rods in PDE6C++ and rd1/+ rods are shown in Figure 4A. Two differences are observed when comparing these responses. First, the average normalized dim flash response appears accelerated, with a faster rising and recovery phase (Fig. 4B). In addition, the dark current of PDE6C++ rods was lower on average compared with rd1/+ rods on the order of ~6 pA. Response parameters are provided in Table 1. Second, responses in PDE6C++ rods were

**Table 1. Properties of the photoresponse in *rd1/+* and PDE6C++ rods**

| | $I_{1/2}$ ($R^*$/rod) | $R_{max}$ (pA) | Time-to-peak (ms)[a] | Collecting area ($\mu m^2$) | $\tau_{rec}$ (ms) | $\tau_{sat}$ (ms) |
|---|---|---|---|---|---|---|
| *rd1/+* DA | 17 ± 0.7 (9) | 30 ± 1.9 (9) | 220 ± 98 (7) | 0.43 ± 0.02 (7) | 160 ± 14 (7) | 220 ± 9.3 (7) |
| PDE6C++ DA | 25 ± 1.2 (10) | 24 ± 2.0 (10) | 179 ± 14 (7) | 0.41 ± 0.02 (7) | 110 ± 6.6 (7) | 95 ± 7.9 (7) |
| *rd1/+* 8.4 $R^*$/rod/s | 28 ± 2.5 (5) | 24 ± 2.3 (5) | 210 ± 2.2 (5) | | | |
| *rd1/+* 190 $R^*$/rod/s | 270 ± 19 (5) | 13 ± 0.6 (5) | 160 ± 11 (5) | | | |
| PDE6C++ 190 $R^*$/rod/s | 180 ± 12 (9) | 13 ± 1.0 (9) | 100 ± 5.6 (8) | | | |

Data are presented as mean ± SEM (*n*).

[a]Time-to-peak values are provided for average dim flash responses. Please note that not every light stimulation protocol was performed on every cell.
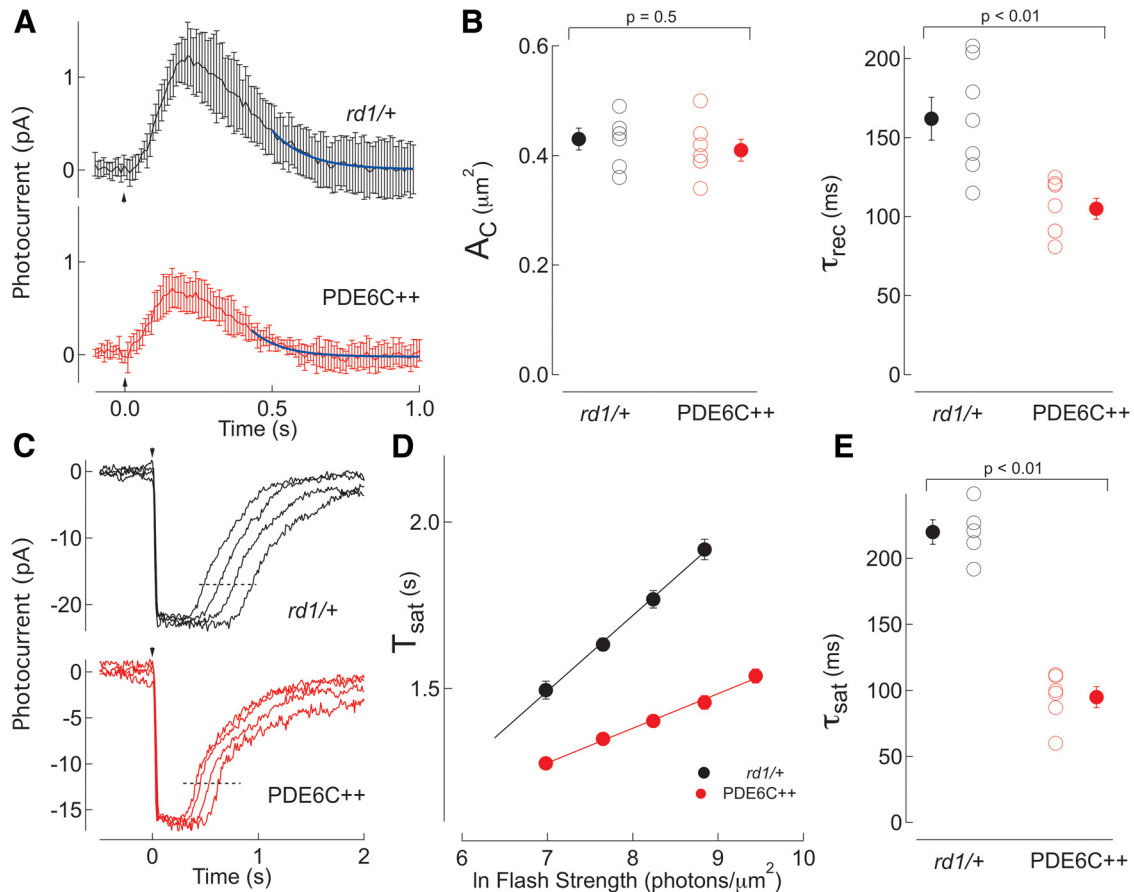


**Figure 5.** Estimate of collecting area and phototransduction deactivation time constant of PDE6C++ and *rd1/+* rods. ***A***, Single-photon responses were derived from the ratio of the time-dependent variance and the mean of the dim flash response (Baylor et al., 1979) and are plotted as a mean and SEM at each time point. Responses were measured with suction electrodes, sampled at 100 Hz, and further low-pass filtered at 20 Hz. The single-photon response from *rd1/+* rods was derived from the sum of 410 dim flash responses (i.e., <25% $R_{max}$) across 7 rods and that from PDE6C++ rods was derived from the sum of 486 dim flash responses across 7 rods. The recovery time constant ($\tau_{rec}$; please refer to the blue fit in the traces) was estimated from the exponential recovery of the final 35% of the single-photon response. ***B***, The collecting area of *rd1/+* and PDE6C++ rods was determined from the scaling factor between the time-dependent variance and the mean of the dim flash response. For *rd1/+* rods, the collecting area was 0.43 ± 0.02 $\mu m^2$ (*n* = 7) and, for PDE6C++ rods, the collecting area was 0.41 ± 0.02 $\mu m^2$ (*n* = 7): not different statistically. The mean $\tau_{rec}$ values for *rd1/+* rods was 160 ± 14 ms (*n* = 7) and for PDE6C++ rods was 110 ± 6.6 ms (*n* = 7), with *p* < 0.01. ***C***, The rate-limiting step for deactivation of rod phototransduction was established using the procedures outlined in Pepperberg et al. (1992). Bright flashes were delivered that hold the rod photocurrent in saturation for increasing periods of time. The time taken for responses to recover 25% of the dark current (dashed line) is denoted. ***D***, The 25% recovery time was plotted against the natural logarithm of the flash strength. The saturation time constant ($\tau_{sat}$) is determined as the slope of this relationship. ***E***, The $\tau_{sat}$ values for *rd1/+* rods was 220 ± 9.3 ms (*n* = 7) and for PDE6C++ rods was 95 ± 7.9 ms (*n* = 7), with *p* < 0.01.

desensitized by ∼1.5-fold (Fig. 4*C*). This desensitization is not caused by a reduction in the quantum catch, or collecting area, in PDE6C++ rods (Fig. 5*B*). However, such speeding and desensitization may be predicted by the higher basal PDE6 activity, and thus the dark rate of cGMP turnover, in PDE6C++ rods. These changes in the light-evoked response are characteristic features of light adaptation, a process by which background light desensitizes photoresponses to prevent response saturation.

We tested the hypothesis that increasing the cGMP turnover rate in *rd1/+* rods would recapitulate to some extent the speeding

and desensitization observed in PDE6C++ rods by applying a weak background light. The background light intensity (8.4 $R^*$/rod/s) was chosen to suppress a small fraction of the dark current equal to the difference in dark current between *rd1/+* and PDE6C++ rods in darkness (Table 1). Background light this weak desensitizes rods by less than a factor of 2 (Dunn et al., 2006). Dim flash responses in *rd1/+* rods measured at this background partially recapitulate the rising phase of the dim flash response (Fig. 4*B*) and the sensitivity of PDE6C++ rods in darkness (Fig. 4*C*).

The recovery of the dim flash response in PDE6C++ rods remained quicker than *rd1/+* rods exposed to background light (Fig. 4B). A more comprehensive characterization of the single-photon response (SPR) in *rd1/+* and PDE6C++ rods is shown in Figure 5A, where SPRs were derived from the ratio of the time-dependent variance and mean of dim flash responses in the linear range (Baylor et al., 1979). From these derived SPRs, we determined the recovery time constant ($\tau_{rec}$) from the single exponential fit of the final phase of the recovery. In PDE6C++ rods, $\tau_{rec} = 110 \pm 6.6$ ms ($n = 7$ rods) compared with *rd1/+* rods, where $\tau_{rec} = 160 \pm 13$ ms ($n = 7$ rods), as shown in Figure 5B. The shorter recovery time constant is consistent with the faster deactivation of the phototransduction cascade. We also measured the deactivation rate of the phototransduction cascade using methods developed by Pepperberg et al. (1992), which have shown previously that the rate-limiting step for shutoff of the phototransduction cascade in dark-adapted mouse rods is the deactivation of PDE6 (Krispel et al., 2006). In Figure 5C, we used suction electrode recordings to measure the response of rods to bright flashes that hold the OS photocurrent in saturation for various durations. The slope of the linear relationship between the time spent in saturation and the natural logarithm of the flash strength is the rate-limiting time constant ($\tau_{sat}$; Pepperberg et al., 1992). In PDE6C++ rods, $\tau_{sat} = 95 \pm 7.9$ ms ($n = 6$ rods) compared with *rd1/+* rods, where $\tau_{sat} = 220 \pm 9.3$ ms ($n = 5$ rods). Therefore, PDE6C is capable of ~2.3-fold faster deactivation than PDE6AB.

To probe the effects of combined action of faster PDE6 deactivation and higher basal cGMP hydrolysis rates, we simulated SPRs of *rd1/+* and PDE6C++ rods using the RodSim program and the model of phototransduction described by Nikonov et al. (2000). The parameter values for *rd1/+* SPR simulations were allowed to vary near the generally accepted values (Gross et al., 2012), except that $\tau_{rec}$ was set to the experimentally derived value of 160 ms. The key features of the *rd1/+* SPR, such as the amplitude and time-to-peak, were then broadly reproduced in a simulation requiring the rate of basal cGMP hydrolysis of 1.7 s$^{-1}$ (Fig. 6). With $\tau_{rec}$ adjusted to the experimentally derived value of 110 ms, the PDE6C++ SPR is closely simulated with concomitant increase in basal cGMP hydrolysis to 2.0 s$^{-1}$. Importantly, only the change in basal PDE6 activity, but not in $\tau_{rec}$, also leads to a decrease in the dark current. Therefore, the combined action of the faster deactivation and the higher basal cGMP hydrolysis rate can largely account for the changes in kinetics and sensitivity of PDE6C++ rods.

### Background light desensitizes *rd1/+* rods to a greater extent than PDE6C++ rods

To assess how increased light-driven, or steady, PDE6 activity influences light adaptation, we exposed *rd1/+* and PDE6C++ rods to a brighter background light that yielded ~190 R*/rod/s. At this background light intensity, the dark currents of these rods were similar (Table 1), but the effects on the sensitivity and time course of flash responses were varied. Flash response families shown in Figure 7A reveal that responses in PDE6C++ rods displayed speeded onset and recovery kinetics compared with their *rd1/+* counterparts (Fig. 7B), but were not desensitized to the same extent (Fig. 7C). PDE6C++ rods were desensitized ~7-fold compared with darkness ($I_{1/2} = 180 \pm 12$ R*; $n = 9$), but *rd1/+* rods were desensitized ~16-fold ($I_{1/2} = 270 \pm 19$ R*; $n = 5$). These background-induced changes ultimately made *rd1/+* rods less sensitive than PDE6C++ rods in background light, essentially reversing the relationship observed in darkness. To
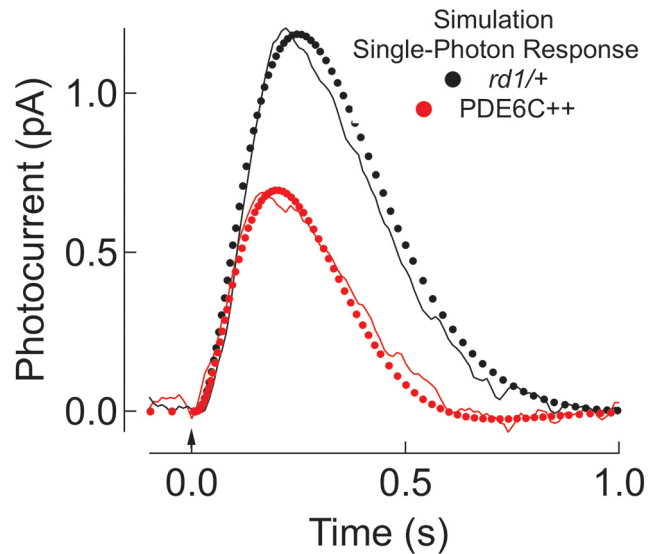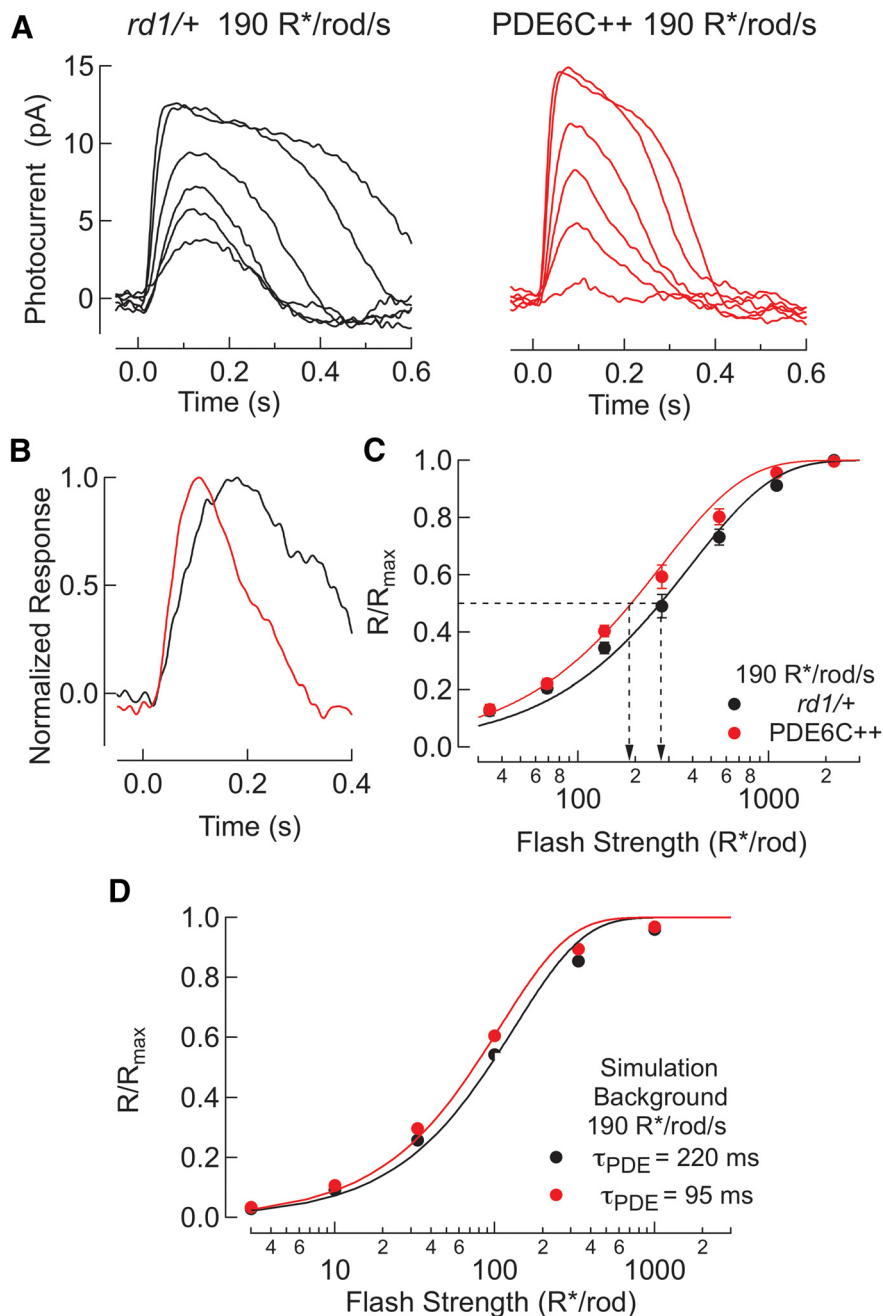


**Figure 6.** Simulated responses of *rd1/+* and PDE6C++ rods. The simulated SPR for *rd1/+* (black dotted line) and PDE6C++ rods (red dotted line) are overlaid with the experimentally derived SPRs, which have been further low-pass filtered at 20 Hz. With $\tau_{rec}$ set at 160 ms (Table 1), the simulated SPR broadly reproduced the *rd1/+* SPR using the following key parameter values: PDE$_{dark}$ = 1.7 s$^{-1}$; amplification constant $A$ = 15 s$^{-2}$; $R^*$ lifetime $\tau_R^*$ = 50 ms; cGMP$_{dark}$ = 5 $\mu$M; Hill coefficients of 3 and 2 for cGMP channel activation and cyclase activation by Ca$^{2+}$, respectively. The PDE6C++ SPR was simulated by varying PDE$_{dark}$ with $\tau_{rec}$ set at 110 ms (Table 1). An agreement with the experimentally derived SPR was achieved by raising PDE$_{dark}$ to 2 s$^{-1}$, which reduced cGMP$_{dark}$ by ~0.2 $\mu$M and the dark current by 2.2 pA.

determine whether the faster deactivation of PDE6C may have contributed to the smaller background-induced desensitization of PDE6C++ rods, we performed additional RodSim simulations of rod response-intensity relationships assuming a background light of 190 R*/rod/s (Fig. 7D). These simulations support qualitatively the idea that the rapid turnoff of PDE6C reduces desensitization in background light by lowering the steady activity of PDE6 (Fig. 7D).

## Discussion

The molecular underpinnings for distinct physiology of rods and cones remain one of the fundamental open questions in photoreceptor biology. Various mechanisms have been suggested for the faster signaling and lower sensitivity of cones, including the activity of rod- and cone-specific components of phototransduction and OS structure (Fu and Yau, 2007; Arshavsky and Burns, 2012; Korenbrot, 2012). Of particular interest has been the role of the effector enzyme, the rod and cone PDE6, because their dark- and light-induced activity is critical in setting the cGMP turnover rate in the OS, and thus the properties of photoresponses (Rieke and Baylor, 1996; Nikonov et al., 2000). For example, it is well appreciated that the time course of the elementary responses in rods and cones in the same species differ as much as 5-fold (Baylor et al., 1984; Schnapf et al., 1990; Nikonov et al., 2006), necessitating differential control on the cGMP turnover rate. Given the functional similarity of rod and cone visual pigments (Shi et al., 2007) and transducins (Deng et al., 2009; Chen et al., 2010; Mao et al., 2013), the PDE6 effector would seem to be key to playing a prominent role in the observed rod/cone differences.

Both structural and functional differences between cone and rod PDE6 have been described. Cone PDE6 is a catalytic homodimer of two PDE6C (PDE6$\alpha'$) subunits, whereas rod PDE6 is a unique catalytic heterodimer PDE6AB (PDE6$\alpha\beta$). Although both cone and rod PDE6 are prenylated at the C-terminal CAAX

**Figure 7.** Photoresponses of PDE6C++ and rd1/+ rods in steady background light. ***A***, Light-evoked responses of a representative rd1/+ (black) and PDE6C++ (red) rods on a steady background light of 190 R*/rod/s. Flash responses in both rd1/+ and PDE6C++ rods yielded 69, 130, 280, 550, 1000, and 2200 R*/rod. Rod responses were sampled at 1 kHz and further low-pass filtered at 30 Hz. ***B***, Average normalized dim flash response (<25% R$_{max}$) of rd1/+ and PDE6C++ rods on a steady background light of 190 R*/rod/s. The average response was produced by 34 R* in rd1/+ rods (n = 15 responses) and 35 R* in PDE6C++ rods (n = 27 responses). ***C***, Average response-intensity relationship for rd1/+ (black; n = 5) and PDE6C++ (red; n = 9) rods exposed to 190 R*/rod/s. Each dataset was fit with an exponential saturation function (Lamb et al., 1981) from which the I$_{1/2}$ value was extracted. The I$_{1/2}$ values for these fits correspond to 270 R* and 180 R* for rd1/+ and PDE6C++ rods, respectively. Note the reversed position of these curves in background light compared with darkness in Figure 4C. ***D***, Simulation of the effect of accelerated recovery on response-intensity relationships. Rod responses to flashes yielding 3, 10, 33, 100, 333, 1000, and 3333 R*/rod on a steady background light of 190 R*/rod/s were simulated with RodSim. Using PDE$_{dark}$ of 2 s$^{-1}$ and the recovery time constants ($\tau_{PDE}$) of 220 and 95 ms corresponding to the experimentally derived $\tau_{sat}$ values for rd1/+ (black) and PDE6C++ rods (red), the R$_{max}$ values were 10.3 and 12.8 pA and PDE$_{steady}$ was 7.2 and 4.6 s$^{-1}$, respectively. From the exponential saturation fits, I$_{1/2}$ = 93 R*/rod (black) and 74 R*/rod (red).

boxes, the heterodimeric nature of PDE6AB dictates differential prenylation of this enzyme (Anant et al., 1992). Distinct prenylation of rod and cone PDE6 may influence how tightly the enzymes are bound to the membrane, so this may alter the activity

of the membrane-bound complex of G$\alpha_{t1}$ with PDE6 (Catty et al., 1992; Clerc and Bennett, 1992; Malinski and Wensel, 1992). Rod and cone PDE6 also differ in noncatalytic cGMP binding to the regulatory GAF domains (Gillespie and Beavo, 1988, 1989) and display dissimilar activation by transducin in solution (Gillespie and Beavo, 1988; Muradov et al., 2010).

We investigated the potential contribution of PDE6 isoforms to the rod–cone signaling differences in a transgenic mouse model in which PDE6C is expressed in rd1/rd1 rods lacking functional PDE6AB. This model allowed uniform transgene expression and the monitoring of levels of PDE6C protein and activity. Expression of PDE6C in single-transgenic PDE6C+ mice effectively rescued the rd1/rd1 retinal degeneration phenotype in young mice. However, the levels of PDE6C protein and maximal PDE6 activity were significantly lower than in WT or rd1/+ rods. We matched the levels of PDE6C and PDE6AB in mouse rods by generating double-transgenic PDE6C++ mice and using rd1/+ mice as controls. PDE6 activity measurements in PDE6C++ and rd1/+ retinal homogenates indicated about 3-fold higher rate of basal cGMP hydrolysis by PDE6C compared with PDE6AB. The higher basal activity of PDE6C cannot be attributed to different levels of Pγr in PDE6C++ and rd1/+ rods. In addition, the potency of inhibition of trypsin-activated PDE6C and PDE6AB by Pγr were similar and comparable to the potency of PDE6C inhibition by Pγc. Therefore, we surmise that the elevated basal activity of PDE6C is a fundamental property of the membrane-bound holoenzyme. Hypothetically, a different interaction of cone PDE6C with the membrane due to protein geranylgeranylation and/or a distinct protein surface charge (Hurwitz et al., 1985; Anant et al., 1992) may allow the Pγ-subunit to interact with the membrane surface lipids in such a way that leads to more frequent openings of the PDE6C catalytic pocket in darkness. In agreement, high cGMP synthetic activity was measured in dark-adapted carp cones, suggesting that basal PDE6 activity and cGMP turnover are also higher in carp cones compared with rods (Takemoto et al., 2009).

Elevated basal PDE6 activity, and the resulting increase in cGMP turnover rate, coupled with the ~2-fold faster PDE6C deactivation, appears to endow PDE6C++ rods with less sensitive and quicker photoresponses. In the dark-adapted state, PDE6C++ rod photoresponses displayed ~1.5-fold reduced sensitivity and ~20% shorter time-to-peak than in control rd1/+ rods. The higher level of basal PDE6 activity also appears to reduce

the dark current of rods by ~6 pA. To determine how this PDE-dependent reduction in dark current influences photoresponses, we applied a dim background light that suppressed about the same dark current and compared the properties of flash responses delivered on the background. Photoresponses in *rd1/+* rods evoked on a background of 8.4 *R*\*/rod/s reproduce broadly the change in sensitivity and rising phase of photoresponses observed in PDE6C++ rods (Fig. 4). Because background light this weak does not produce substantial desensitization (Dunn et al., 2006), these properties of PDE6C++ rod photoresponses in darkness can be explained largely by the elevation in basal PDE activity and speeded PDE6 deactivation rate.

To test the capacity of PDE6C++ and *rd1/+* rods for light adaptation, we applied a brighter background light of 190 *R*\*/rod/s, a background expected to desensitize the rods by ~10-fold (Dunn et al., 2006). Given the similar collecting area of PDE6C++ and *rd1/+* rods, background lights would be expected to generate similar amounts of *R*\*. Under these circumstances, we find that *rd1/+* rods were desensitized to a far greater degree than their PDE6C++ counterparts, essentially reversing their relative sensitivity in darkness (Figs. 4C vs 7C). The reduced desensitization of PDE6C++ rods is consistent with a smaller increase in steady PDE6C++ activity. Two factors are most likely to contribute to this difference. First, in background light, the steady PDE6 activity is much greater than the basal PDE6 activity observed in darkness. Therefore, the background-induced activity of PDE6C and PDE6AB become more similar and the relative change in sensitivity for rods with a lower basal PDE6 activity (i.e., *rd1/+* with PDE6AB) was larger. Second, the faster deactivation of PDE6C further reduces its steady activity and blunts the background-induced desensitization (Fig. 7D) (Nikonov et al., 2000). Therefore, lower steady PDE6C activity in background light may serve to increase the operational range of PDE6C rods. This mechanism would be expected to contribute to adaptation in cones, which are able to avoid saturation in intense background light (Burkhardt, 1994).

The phenotype of PDE6C++ rods contrasts the recent findings of increased sensitivity and slower response kinetics of *rd10* rods expressing PDE6C after viral-mediated delivery of the transgene (Deng et al., 2013). However, such changes in light responses may not be caused necessarily by molecular attributes of PDE6C, but they can also result from a low level of PDE6C expression in *rd10* rods, which would lead to a reduced spontaneous turnover of cGMP. Analyses of Rieke and Baylor (1996) and Nikonov et al. (2000) demonstrate the key role of the cGMP turnover rate in setting the properties the rod photoresponse. Consistent with this critical role for basal PDE6 activity, AIPL1-hypomorphic rods with low expression of PDE6 show greater photoresponse sensitivity and a longer recovery phase (Makino et al., 2006). Therefore, the physiological properties of rods in the viral delivery model may have been caused by inadequate expression of PDE6C in a background lacking PDE6AB.

In conclusion, our study demonstrates that the increase in basal activity and faster deactivation provided by PDE6C appears to account partially for the difference in the photoresponse properties of rods versus cones. The contribution of other components of the phototransduction cascade, however, is ultimately necessary to account entirely for the fast response and low sensitivity of cones. This work adds to a body of literature showing that multiple components of the phototransduction cascade, including the visual pigment (Kefalov et al., 2003; Sakurai et al., 2007; Shi et al., 2007; Matthews and Sampath, 2010), G-protein (Deng et al., 2009; Chen et al., 2010; Mao et al., 2013), and RGS9 GAP

complex (Cowan et al., 1998; Zhang et al., 2003), contribute synergistically to generate the overall differences in the physiological responses of rods versus cones.

## References

Anant JS, Ong OC, Xie HY, Clarke S, O'Brien PJ, Fung BK (1992) In vivo differential prenylation of retinal cyclic GMP phosphodiesterase catalytic subunits. J Biol Chem 267:687–690. Medline

Arshavsky VY, Burns ME (2012) Photoreceptor signaling: supporting vision across a wide range of light intensities. J Biol Chem 287:1620–1626. CrossRef Medline

Baylor DA, Lamb TD, Yau KW (1979) Responses of retinal rods to single photons. J Physiol 288:613–634. Medline

Baylor DA, Nunn BJ, Schnapf JL (1984) The photocurrent, noise and spectral sensitivity of rods of the monkey Macaca fascicularis. J Physiol 357:575–607. CrossRef Medline

Bryda EC, Bauer BA (2010) A restriction enzyme-PCR-based technique to determine transgene insertion sites. Methods Mol Biol 597:287–299. CrossRef Medline

Burkhardt DA (1994) Light adaptation and photopigment bleaching in cone photoreceptors in situ in the retina of the turtle. J Neurosci 14:1091–1105. Medline

Catty P, Pfister C, Bruckert F, Deterre P (1992) The cGMP phosphodiesterase-transducin complex of retinal rods: membrane binding and subunits interactions. J Biol Chem 267:19489–19493. Medline

Chen CK, Woodruff ML, Chen FS, Shim H, Cilluffo MC, Fain GL (2010) Replacing the rod with the cone transducin subunit decreases sensitivity and accelerates response decay. J Physiol 588:3231–3241. CrossRef Medline

Clerc A, Bennett N (1992) Activated cGMP phosphodiesterase of retinal rods: a complex with transducin alpha subunit. J Biol Chem 267:6620–6627. Medline

Cowan CW, Fariss RN, Sokal I, Palczewski K, Wensel TG (1998) High expression levels in cones of RGS9, the predominant GTPase accelerating protein of rods. Proc Natl Acad Sci U S A 95:5351–5356. CrossRef Medline

Deng WT, Sakurai K, Liu J, Dinculescu A, Li J, Pang J, Min SH, Chiodo VA, Boye SL, Chang B, Kefalov VJ, Hauswirth WW (2009) Functional interchangeability of rod and cone transducin alpha-subunits. Proc Natl Acad Sci U S A 106:17681–17686. CrossRef Medline

Deng WT, Sakurai K, Kolandaivelu S, Kolesnikov AV, Dinculescu A, Li J, Zhu P, Liu X, Pang J, Chiodo VA, Boye SL, Chang B, Ramamurthy V, Kefalov VJ, Hauswirth WW (2013) Cone phosphodiesterase-6alpha' restores rod function and confers distinct physiological properties in the rod phosphodiesterase-6beta-deficient rd10 mouse. J Neurosci 33:11745–11753. CrossRef Medline

Dunn FA, Doan T, Sampath AP, Rieke F (2006) Controlling the gain of rod-mediated signals in the mammalian retina. J Neurosci 26:3959–3970. CrossRef Medline

Fu Y, Yau KW (2007) Phototransduction in mouse rods and cones. Pflugers Arch 454:805–819. CrossRef Medline

Fu Y, Kefalov V, Luo DG, Xue T, Yau KW (2008) Quantal noise from human red cone pigment. Nat Neurosci 11:565–571. CrossRef Medline

Gillespie PG, Beavo JA (1988) Characterization of a bovine cone photoreceptor phosphodiesterase purified by cyclic GMP-Sepharose chromatography. J Biol Chem 263:8133–8141. Medline

Gillespie PG, Beavo JA (1989) cGMP is tightly bound to bovine retinal rod phosphodiesterase. Proc Natl Acad Sci U S A 86:4311–4315. CrossRef Medline

Gross OP, Pugh EN Jr, Burns ME (2012) Spatiotemporal cGMP dynamics in living mouse rods. Biophys J 102:1775–1784. CrossRef Medline

Hamilton SE, Prusti RK, Bentley JK, Beavo JA, Hurley JB (1993) Affinities of bovine photoreceptor cGMP phosphodiesterases for rod and cone inhibitory subunits. FEBS Lett 318:157–161. CrossRef Medline

Hurwitz RL, Bunt-Milam AH, Chang ML, Beavo JA (1985) cGMP phosphodiesterase in rod and cone outer segments of the retina. J Biol Chem 260:568–573. Medline

Kefalov V, Fu Y, Marsh-Armstrong N, Yau KW (2003) Role of visual pigment properties in rod and cone phototransduction. Nature 425:526–531. CrossRef Medline

Korenbrot JI (2012) Speed, sensitivity, and stability of the light response in

rod and cone photoreceptors: facts and models. Prog Retin Eye Res 31: 442–466. CrossRef Medline

Krispel CM, Chen D, Melling N, Chen YJ, Martemyanov KA, Quillinan N, Arshavsky VY, Wensel TG, Chen CK, Burns ME (2006) RGS expression rate-limits recovery of rod photoresponses. Neuron 51:409–416. CrossRef Medline

Lamb TD, McNaughton PA, Yau KW (1981) Spatial spread of activation and background desensitization in toad rod outer segments. J Physiol 319:463–496. CrossRef Medline

Liebman PA, Evanczuk AT (1982) Real time assay of rod disk membrane cGMP phosphodiesterase and its controller enzymes. Methods Enzymol 81:532–542. CrossRef Medline

Majumder A, Pahlberg J, Boyd KK, Kerov V, Kolandaivelu S, Ramamurthy V, Sampath AP, Artemyev NO (2013) Transducin translocation contributes to rod survival and enhances synaptic transmission from rods to rod bipolar cells. Proc Natl Acad Sci U S A 110:12468–12473. CrossRef Medline

Makino CL, Wen XH, Michaud N, Peshenko IV, Pawlyk B, Brush RS, Soloviev M, Liu X, Woodruff ML, Calvert PD, Savchenko AB, Anderson RE, Fain GL, Li T, Sandberg MA, Dizhoor AM (2006) Effects of low AIPL1 expression on phototransduction in rods. Invest Ophthalmol Vis Sci 47: 2185–2194. CrossRef Medline

Malinski JA, Wensel TG (1992) Membrane stimulation of cGMP phosphodiesterase activation by transducin: comparison of phospholipid bilayers to rod outer segment membranes. Biochemistry 31:9502–9512. CrossRef Medline

Mao W, Miyagishima KJ, Yao Y, Soreghan B, Sampath AP, Chen J (2013) Functional comparison of rod and cone Galpha(t) on the regulation of light sensitivity. J Biol Chem 288:5257–5267. CrossRef Medline

Matthews HR, Sampath AP (2010) Photopigment quenching is Ca2+ dependent and controls response duration in salamander L-cone photoreceptors. J Gen Physiol 135:355–366. CrossRef Medline

Muradov H, Boyd KK, Artemyev NO (2006) Analysis of PDE6 function using chimeric PDE5/6 catalytic domains. Vision Res 46:860–868. CrossRef Medline

Muradov H, Boyd KK, Artemyev NO (2010) Rod phosphodiesterase-6 PDE6A and PDE6B subunits are enzymatically equivalent. J Biol Chem 285:39828–39834. CrossRef Medline

Nikonov SS, Kholodenko R, Lem J, Pugh EN Jr (2006) Physiological features of the S- and M-cone photoreceptors of wild-type mice from single-cell recordings. J Gen Physiol 127:359–374. CrossRef Medline

Nikonov S, Lamb TD, Pugh EN Jr (2000) The role of steady phosphodiesterase activity in the kinetics and sensitivity of the light-adapted salamander rod photoresponse. J Gen Physiol 116:795–824. CrossRef Medline

Okawa H, Sampath AP, Laughlin SB, Fain GL (2008) ATP consumption by mammalian rod photoreceptors in darkness and in light. Curr Biol 18: 1917–1921. CrossRef Medline

Okawa H, Miyagishima KJ, Arman AC, Hurley JB, Field GD, Sampath AP (2010) Optimal processing of photoreceptor signals is required to maximize behavioural sensitivity. J Physiol 588:1947–1960. CrossRef Medline

Pahlberg J, Sampath AP (2011) Visual threshold is set by linear and nonlinear mechanisms in the retina that mitigate noise How neural circuits in the retina improve the signal-to-noise ratio of the single-photon response. Bioessays 33:438–447. CrossRef Medline

Pepperberg DR, Cornwall MC, Kahlert M, Hofmann KP, Jin J, Jones GJ, Ripps H (1992) Light-dependent delay in the falling phase of the retinal rod photoresponse. Vis Neurosci 8:9–18. CrossRef Medline

Rieke F, Baylor DA (1996) Molecular origin of continuous dark noise in rod photoreceptors. Biophys J 71:2553–2572. CrossRef Medline

Sakurai K, Onishi A, Imai H, Chisaka O, Ueda Y, Usukura J, Nakatani K, Shichida Y (2007) Physiological properties of rod photoreceptor cells in green-sensitive cone pigment knock-in mice. J Gen Physiol 130:21–40. CrossRef Medline

Sakurai K, Chen J, Kefalov VJ (2011) Role of guanylyl cyclase modulation in mouse cone phototransduction. J Neurosci 31:7991–8000. CrossRef Medline

Schnapf JL, Nunn BJ, Meister M, Baylor DA (1990) Visual transduction in cones of the monkey Macaca fascicularis. J Physiol 427:681–713. CrossRef Medline

Shi G, Yau KW, Chen J, Kefalov VJ (2007) Signaling properties of a short-wave cone visual pigment and its role in phototransduction. J Neurosci 27:10084–10093. CrossRef Medline

Sinha S, Majumder A, Belcastro M, Sokolov M, Artemyev NO (2013) Expression and subcellular distribution of UNC119a, a protein partner of transducin alpha subunit in rod photoreceptors. Cell Signal 25:341–348. CrossRef Medline

Sokolov M, Strissel KJ, Leskov IB, Michaud NA, Govardovskii VI, Arshavsky VY (2004) Phosducin facilitates light-driven transducin translocation in rod photoreceptors: evidence from the phosducin knockout mouse. J Biol Chem 279:19149–19156. CrossRef Medline

Stec DE, Morimoto S, Sigmund CD (2001) Vectors for high-level expression of cDNAs controlled by tissue-specific promoters in transgenic mice. Biotechniques 31:256–258,260. Medline

Takemoto N, Tachibanaki S, Kawamura S (2009) High cGMP synthetic activity in carp cones. Proc Natl Acad Sci U S A 106:11788–11793. CrossRef Medline

Tsang SH, Gouras P, Yamashita CK, Kjeldbye H, Fisher J, Farber DB, Goff SP (1996) Retinal degeneration in mice lacking the gamma subunit of the rod cGMP phosphodiesterase. Science 272:1026–1029. CrossRef Medline

Tsang SH, Burns ME, Calvert PD, Gouras P, Baylor DA, Goff SP, Arshavsky VY (1998) Role for the target enzyme in deactivation of photoreceptor G protein in vivo. Science 282:117–121. CrossRef Medline

Zhang X, Wensel TG, Kraft TW (2003) GTPase regulators and photoresponses in cones of the eastern chipmunk. J Neurosci 23:1287–1297. Medline